Computational Materials Science 184 (2020) 109936

Contents lists available at ScienceDirect

Computational Materials Science

journal homepage: www.elsevier.com/locate/commatsci

Solution combustion synthesis and Monte Carlo simulation of the formation of CuNi integrated nanoparticles

Nickolay Sdobnyakov[a], Alexander Khort[b,c,*], Vladimir Myasnichenko[a], Kirill Podbolotov[c,d], Elena Romanovskaia[e], Andrey Kolosov[a], Denis Sokolov[a], Valentin Romanovski[c,f,*]

[a] Tver State University, Sadovii per., 35, 170100 Tver, Russia
[b] KTH, Royal Institute of Technology, Drottning Kristinas vag 51, SE-100 44 Stockholm, Sweden
[c] Center of Functional Nano-Ceramics, National University of Science and Technology «MISIS», Leninsky pr. 4, 119049 Moscow, Russia
[d] Physical-Technical Institute, National Academy of Sciences of Belarus, 220141 Minsk, Belarus
[e] Belarusian State Technological University, 220006, Sverdlova, 13a, Minsk, Belarus
[f] Institute of General and Inorganic Chemistry, National Academy of Sciences of Belarus, Surganova 9/1, 220072 Minsk, Belarus

ARTICLE INFO

Keywords:
Cu-Ni nanoparticle
Solution combustion synthesis
Coalescence
Computer simulation
Gupta potential
Monte-Carlo method

ABSTRACT

The fine bimetallic Cu-Ni integrated nanoparticles were obtained by the modified solution combustion synthesis in the air using glycine as a fuel. The synthesized nanoparticles were studied by XRD analysis using single- and two-phase approaches for Rietveld refinement simulation, by scanning TEM–EDX spectroscopy and HR TEM technics. The data analysis for nanoparticles' characteristics showed close integration of Cu and Ni crystalline structures, which tend to form a bimetallic alloy. The process of bimetallic nanoparticles' formation was computer simulated using the Monte Carlo method in the temperature range from 300 to 600 K. The simulation established the patterns of neck formation for two cases of the initial arrangement of copper and nickel nanoparticles: direct contact and relative displacement of 0.2 nm. It was established, that in the case of relative displacement in comparison with the case of the direct contact the coalescence process is «delayed» by 60–80 K upon heating. A description of the energy spectra of two particles during the neck forming has been provided.

1. Introduction

The interest of researchers to metal nanoparticles is high due to the prospects for their practical application, mostly biological [1–3] and in catalysis [4–6], and the presence of size-related effects, i.e., the difference between their properties and the characteristics of the corresponding bulk phase. These areas of research are expanding thanks to the development of new approaches to nanoparticles synthesis and modification. The using size-related effects closely interconnect practical and scientific aspects of interest to metal nanoparticles.

The transition from single-component metal nanoparticles to binary and multicomponent nanomaterials significantly expands both the range of structural transformations associated with them and the prospects for their practical application. In particular, the binary and multicomponent nanoparticles are characterized by the phenomenon of surface segregation – the process of enrichment of nanoalloy surface region by one of the components of a nanoalloy as a result of diffusion of that element from the internal volume of the nanoparticle to the surface region [7]. The segregation in nanoparticles manifests in the evolution of the system at a constant and changing temperatures. The coalescence phenomenon – the process of the merging of two or more nanoparticles into one phase – can serve as an approach for producing binary and multicomponent nanoparticles [8,9]. Understanding factors that influence the binary coalescence rates in the various sintering, which is the process of compacting and forming a solid phase of nanomaterial without melting it to the point of liquefaction, caused by external factors, could significantly improve the quality of the final product and make their production more effective. There were made multiple efforts to compile theoretical modeling and experimental approaches to the phenomena studying [10]. The computer simulation methods, in particular the Monte Carlo method, have been sufficiently tested in studying the processes of sintering/coalescence, before [11]. It was confirmed [12], that viscosity and particle size influence particles' behavior overall, including melting, while morphology and porosity do not impact particle coalescence, significantly. However, the structural changes in the neck between particles during coalescence were not

* Corresponding authors at: KTH, Royal Institute of Technology, Drottning Kristinas vag 51, SE-100 44 Stockholm, Sweden (A Khort) and Center of Functional Nano-Ceramics, National University of Science and Technology «MISIS», 119049, Moscow, Russia (A Khort and V Romanovski).
E-mail addresses: khort@kth.se (A. Khort), vramano@kth.se (V. Romanovski).

https://doi.org/10.1016/j.commatsci.2020.109936
Received 13 May 2020; Received in revised form 10 July 2020; Accepted 11 July 2020
Available online 21 July 2020

studied sufficiently before. While the nanostructured hollow Ni particle synthesis technology and the study of fcc/hcp transformations were proposed without consideration of the sintering mechanism [13].

The Cu-Ni bimetallic system is known for antibacterial activity [14,15], as a catalyst for selective hydrogenolysis of glycerol [16], furfural conversion [17], degradation of organic dyes [18], selective hydrogenation of p-nitrophenol and cinnamaldehyde [19], hydrodeoxygenation of vanillin [20], cyanation of aryl halides [21], CO_2 reforming of methane [22]. It could be found different ways for synthesis Cu-Ni nanoparticles: hydrothermal [18,23], by a microemulsion route using cetyl trimethyl ammonium bromide as the surfactant [24], mechanical milling [25], different precipitation methods [26,27], solvothermal method [28] or prepared via microemulsion [29]. According to the experimental data [30], there is pronounced surface segregation of Cu to the surface of the bulk Cu-Ni alloy. Thus, the study of the synthesis of Cu-Ni nanoparticles experimentally and with the use of computer simulation results is an urgent task. In particular, such attempts have already been made to study segregation in the Cu-Ni system [31]. However, in this work, the simulation took place at a temperature of 100 K, but the experimental conditions corresponded to a temperature of 573 K. Such significant temperature differences, in our opinion, do not fully allow us to compare the results of the experiment and computer simulation correctly. Although, the use of the hybrid molecular dynamics/Metropolis Monte Carlo algorithm based on the embedded atom method suggests a high degree of realism of the simulation results. For calculation of the value of the total potential energy of nanoparticles, the Gupta potential was used. This potential, as well as the parameters, given in [32], were tested to a sufficient degree and compared with the results of using the parameters for the tight-binding potential, using DFT calculations [33]. However, one should take into account, DFT calculations were not adequately tested in a wide range of nanoparticle sizes. It is evident, that the analysis of phase and structural transformations is complicated, and requires careful selection of the model interaction potential for each component and, in particular, for cross-parameters.

As a method for particles' synthesis for this work, we chose the solution combustion synthesis (SCS) as a prospective method in terms of time, reagents, and environmental impact [34]. SCS is a highly exothermic reaction of an oxidation-reduction mixture. Using precursors in the form of solutions gives an advantage in a homogeneous composition on a molecular level. Such type of reaction can provide a synthesis of metal nanoparticles even in the air atmosphere due to the large number of gaseous products that prevent formed metals from oxidation [35].

The objectives of this study were to *i*) compare experimental data for Cu-Ni synthesis with Monte-Carlo simulation results, and *ii*) to estimate the dihedral angle for Cu-Ni neck and temperature stages of the coalescence process. It was accomplished by combining methodologies from our previous researches [8,9], and different surface and materials characterization techniques. The results of the research can be useful in predicting temperature ranges for the synthesis of nanoscale active and passive elements for nanoelectronics, which have a certain set of physical characteristics, taking into account their size dependences.

2. Experimental

2.1. Materials

All chemicals were the analytical-grade reagents and used without any further purification. Nickel nitrate hexahydrate ($Ni(NO_3)_2{\cdot}6H_2O$) and copper nitrate trihydrate ($Cu(NO_3)_2{\cdot}3H_2O$) were used as metal precursors, glycine ($C_2H_5NO_2$, G) as reducing reagent.

2.2. Synthesis procedure

Ni-Cu NPs sample with Ni to Cu molar ratios of 1:1 was synthesized by a modified SCS approach [36–38] using a water solution of metal nitrates (oxidizer) and G (fuel). The fuel-to-oxidizer ratio φ was kept 1.75, which was chosen based on our previous researches [39,40]. In the case of $\varphi > 1$, CO_2 and N_2 rich protective gas media forms in a reactor volume. This provides the possibility of obtaining pure metal under air as an external atmosphere.

The sample was prepared as follows. Stichometrical amounts of metal nitrates were dissolved in the minimum amount of hot distillate water. Then the appropriate amount of G was added to get required φ, according to SCS reactions in Eq. (1):

$$Cu(NO_3)_2 + Ni(NO_3)_2 + (8/3\ \varphi)\ C_2H_5NO_2 + 6(\varphi - - 1)\ O_2 = CuNi + (16/3\ \varphi)CO_2 + ((4\varphi + 6)/3)N_2 + (20/3\ \varphi)H_2O \quad (1)$$

The obtained solution was drying rapidly in microwave furnace (800 W, 2.450 GHz) until gel and then foam has formed. The foam was ignited and burned in a preheated muffle furnace at 873 K under normal air atmosphere, leading to the formation of a fluffy powder, which was removed from the furnace after reaction completion and rapidly cooled in a closed crucible to prevent metal oxidation. The protective or reducing atmospheres were not used.

Table 1
Gupta's parameters used in the calculations.

Component binding	A, eV	ζ, eV	p	q	r_0, Å
Ni-Ni	0.0376	1.070	16.999	1.189	2.491
Cu-Cu	0.0855	1.2240	10.960	2.2780	2.556
Ni-Cu	0.06155	1.147	13.9795	1.7335	2.5235

2.3. Characterization

The time-temperature profile of the SCS of the precursor was studied using a home-made setup. The precursors in the form of dried foam were placed in a preheated 350 ± 10 °C vertical muffle furnace in a special alumina crucible with a K-type thermocouple. The output signal of the thermocouple was collected by a data acquisition system.

The thermal evaluation of SCS of experimental systems was conducted by thermal gravimetric analysis (TG) (NETZSCH STA 449 F3 Jupiter). For TG measurement twenty milligrams of the sample in the form of a dried gel was heated in an air atmosphere, at 10 °C per minute up to 760 °C.

The phase composition and crustal structure of the obtained combustion products were characterized by X-ray diffraction (XRD) analysis using Bruker D8 ADVANCE diffractometer with a rotating copper anode CuKα radiation. Rietveld refinements were conducted with the software HighScore Plus. The Pseudo-Voigt function was used for the peak profile refinement. The average crystallite size was determined from the broadening of the diffraction peak using the Scherrer formula $D = K\lambda/\beta\cos\theta$ where D is the average particle size in nm, K is the Scherrer constant (0.89), λ is the wavelength of the X-ray source, β is the full width at half-maximum and θ is the Bragg's angle.

The surface morphology and surface composition were examined using a scanning electron microscope (SEM) with backscattered electron analysis (Tescan Mira 3, Czech Republic) coupled with energy X-ray dispersive spectroscopy (EDS).

Transmission electron microscopy (TEM) images were taken on a JEM-2100F microscope equipped with EDAX Genesis XM 460 system. Samples for TEM were prepared by deposition and drying of a drop (10 μL) of the material dispersed in ethanol onto a carbon-coated 400 mesh copper grid. Image processing was performed in the ImageJ software.

2.4. Monte-Carlo simulation technique and initial configuration

The coalescence/sintering of copper and nickel nanoparticles

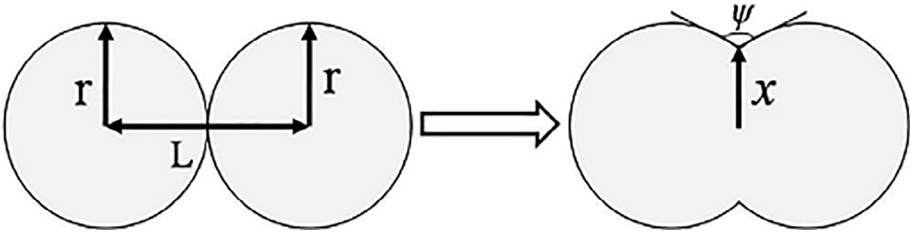

Fig. 1. Scheme of the coalescence of two spherical particles: r is the particle radius, L is the distance between centers of particles, x is the neck radius; ψ is the dihedral angle.

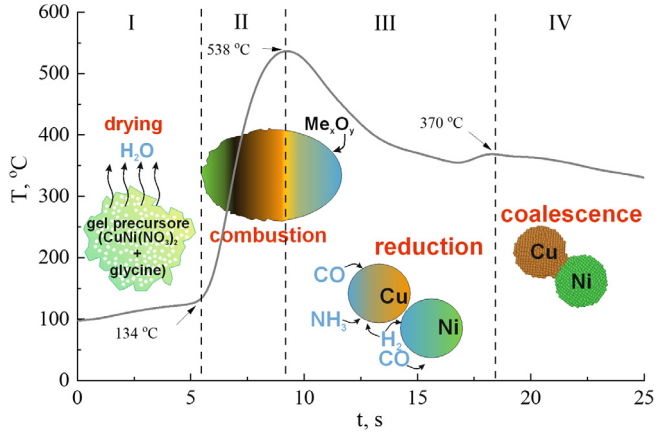

Fig. 2. Time-temperature profile of SCS and simplify scheme of bimetallic particle formation.

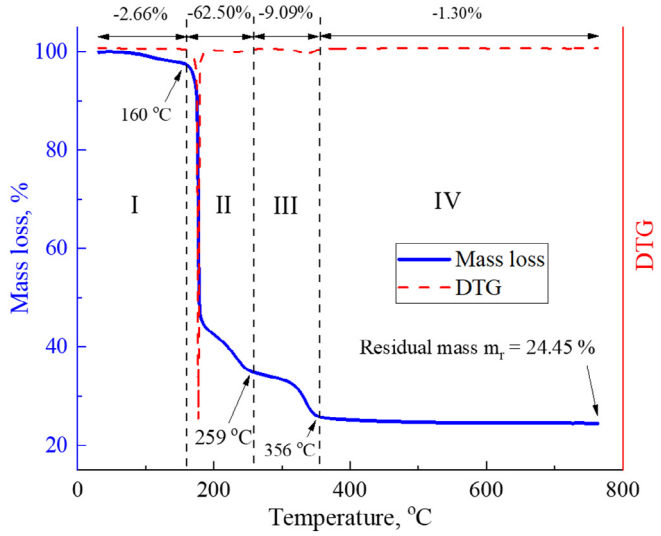

Fig. 3. TG-DTG curves of SCS of (CuNi) nitrates–glycin system in the air.

subjected to gradual heating is simulated using the Monte Carlo simulation method [41]. The interaction of nanoparticles is described using the Gupta many-body potential [42] with parameters from [32]. The standard Monte Carlo simulations without local minimization, but with random local displacements were performed. The simulations consisted of ~$2.8{\cdot}10^8$ single Monte Carlo steps. The value of the total potential energy of nanoparticles containing N metal atoms in the case of using the Gupta potential is given by the expression:

$$U = \sum_{i=1}^{N} U_i,\ U_i = \sum_{j,r_{ij}\le r_c}^{N} A_{ij}exp\left(-p\left(\frac{r_{ij}}{r_{0ij}}-1\right)\right) - \sqrt{\sum_{j,r_{ij}\le r_c}^{N} \varsigma_{ij}^2 exp\left(-2{\cdot}q\left(\frac{r_{ij}}{r_{0ij}}-1\right)\right)}. \quad (2)$$

Here r_{ij} is the distance between the atoms i and j in the cluster, the parameter A_{ij} is the experimental value of cohesion energy, r_{0ij} is the lattice parameter, p and q are values of the elastic constants of the crystal structure at $T = 0$ K. The parameter ς_{ij} depends only on the selected type of atoms. For calculation total potential energy of nanoparticles U, an appropriate cutoff distance r_c was used. In this work, r_c was taken equal to the five-neighbor distance in the respective bulk solids for homogeneous pairs, whereas for heterogeneous pairs the r_c is the arithmetic average.

There are a large number of works devoted to the problem of restoring the metal potential [42–44]. The Gupta many-body potential (tight-binding potential) and its derivatives are widely used to describe the interaction of atoms [32]. It should be noted that the Gupta potential was obtained in the framework of the theory of the density function concerning the cohesion energy of metal atoms and describes the interaction in terms of local electron density. The potential parameters of the interatomic interaction that were used in this series of computer experiments by the Monte Carlo method are presented in Table 1.

Recently, the method of the weight function has been used quite often to find the cross parameters of the potential [45]:

$$P(A-B) = \omega{\cdot}P(A-A) + (1-\omega){\cdot}P(B-B) \quad (3)$$

where P is the Gupta potential parameter, ω is the weight coefficient, A and B indicate the type of metal. In our case, $\omega = 0.5$ is accepted value.

To predict possible structural transformations of the nanosystem of individual Cu-Ni grain pair in the selected temperature range (300–600 K, corresponding to the experimental synthesis conditions), modeling was carried out for a system of spherical nanoparticles Cu_{2315}-Ni_{2491} cut of 5 nm in diameter from an *fcc* massive phase. The size and shape choices are caused by the natural limitations of mathematical apparatus used and reasonable limitation of machine time required for the modeling. For instance, even a small increase in the size of particles leads to a significant increase in computation time. At the same time, the contact spot size, atom diffusion rate, and rate of local crystal lattice formation are not affected by the particles' sizes. Moreover, the coalescence process starts on small particles first, and unique/fundamental patterns most likely can be found in these size level. Using spherical shape particles with the same sizes allows us to avoid the uncertain effect of dimensional factors associated with different kinetics of interaction, vapor densities, and gradients of atomic concentrations.

Two cases are considered that correspond to the contact of particles at the beginning of the simulation and the initial distance of 0.2 nm. Initially, Ni and Cu nanoparticles were placed on the left and right sides of the nanosystem, respectively. For a better touch area and a change in lattice orientation, the copper particle was rotated 45° relative to the nickel particle. 300 K was taken as the initial temperature for modeling, while the upper boundary of the simulation corresponded to a temperature of about 600 K, which can be compared with the data of [31]. At each temperature step, the relaxation of the nanosystem was performed. According to [8], it is possible to calculate the driving force of coalescence and define the onset of particle growth via coalescence, by measuring a dihedral angle at the neck. In the equilibrium state, the dihedral angle can be expressed as follows

$$\gamma_{gb} = 2\gamma_s{\cdot}\cos(\psi/2) \quad (4)$$

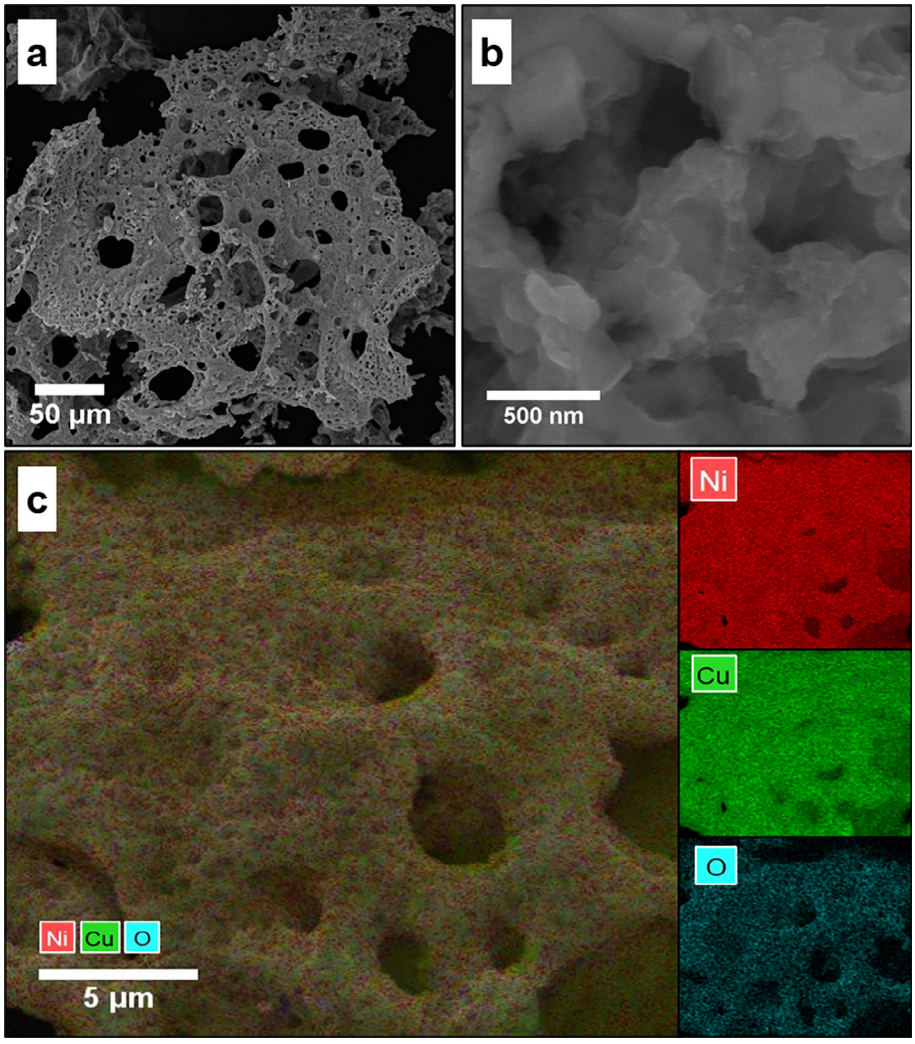

Fig. 4. (a, b) The SEM images and (c) the results of the EDS element mapping of the SCS Cu-Ni sample.

where γ_{gb} is the energy of the grain boundary and γ_s is the surface energy. In the case under consideration, the neck growth proceeds as long as $\psi < \psi_{eq}$, while the growth by grain boundary motion proceeds until the dihedral angle will reach its equilibrium value, which is attained at the final stage of coalescence (sintering).

The scheme presented in Fig. 1 gives the general definition for the dihedral angle in the coalescence of two spherical particles.

The methodology for determining the dihedral angle and the description of the coalescence stages were described in detail earlier [46,47]. In our case, the geometric parameters of nanoparticles (individual agglomerates) in the experimental images of the surface of the images (see parameters described in Fig. 1), and the estimate of the γ_{gb}/γ_s, the relationship could be used as the comparison parameters of the experimental data for Cu-Ni synthesis and Monte-Carlo simulation.

3. Results and discussion

3.1. Solution combustion synthesis of Cu-Ni powder

The time-temperature profile of the SCS process and simplified scheme of bimetallic nanoparticles formation are shown in Fig. 2.

According to methodology, suggested in [48], the SCS process could be divided into 4 separate stages with an ignition temperature of 134 °C and maximal combustion temperature of 538 °C and represented as a complex of exothermic decomposition reactions of organic fuel and metals nitrate with the formation of metals oxide and a mixture of gases, like nitrogen, carbon dioxide, H_2O and others. In this case, an excess of reducing agent, which, due to thermal decomposition, forms an inert or even reduction atmosphere in reaction volume over freshly synthesized metal oxide nanoparticles. This leads to the reduction of metal oxide to pure metal, at certain conditions, and additionally prevents oxidation of the metal by atmospheric oxygen. The high-temperature fast exothermic reaction could create conditions, where nanoparticles of different structure and morphology form [49], including possible interaction of already formed metal crystals, accompanied by their interdiffusion or alloying.

TG-DTG analysis of combustion reaction in the air was implemented to closer study features of SCS of CuNi nanopowders (Fig. 3).

The same four stages could be distinguished in TG-DTG curves. At the first stage (drying), the residual solvent is evaporated. Here only 2.66% weight loss reduction was detected. During drying by the same regime in a muffle oven or microwave oven usually, a foam formation is observed. The exothermic reaction – second (ignition) stage – starts at about 160 °C. At this stage fuels and nitrates start to decompose with gas evaluation, mostly carbon and nitrogen oxides, and water vapor, resulting in the mass loss of 62.5%. Solid phases start to form and mostly finished at this stage. The main resultant products are Cu and Ni oxides, as well as a gas mixture of CO_2, CO, N_2O, and NH_3.

Residual nitrates and fuels decompose, as well as formations of the solid phases, are finished during afterburning (stage three). This results in a mass loss of 9.09%. It is commonly believed, that reduction of freshly synthesized metal oxides to metals occurred mostly at this stage.

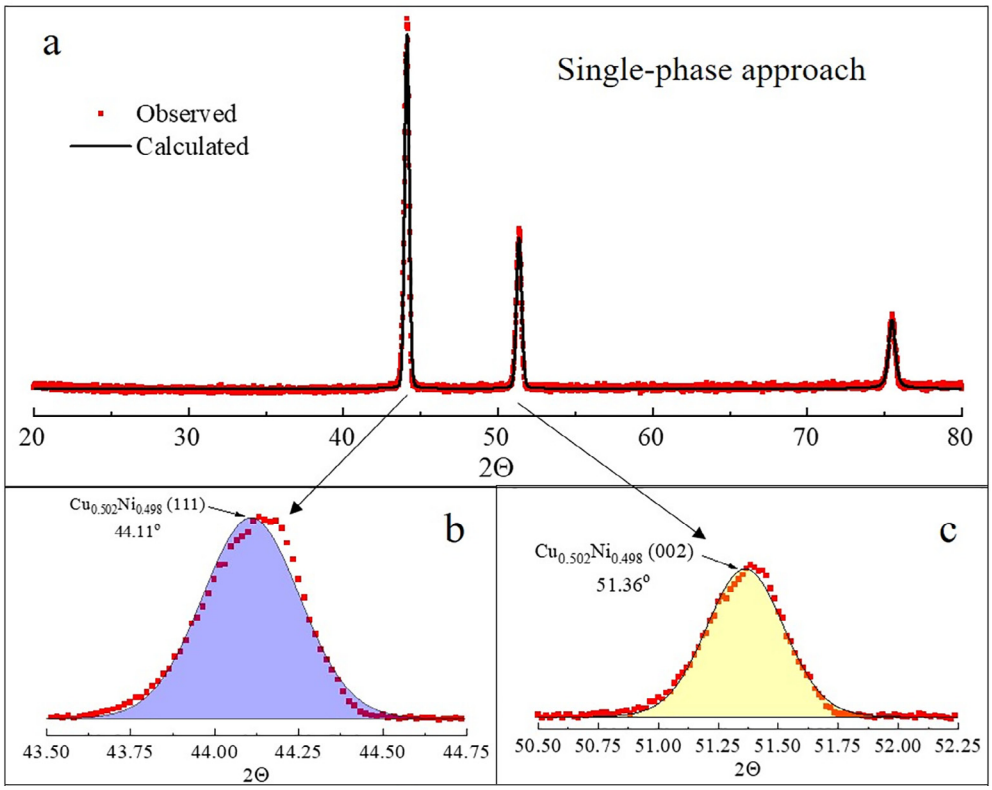

Fig. 5. Results of XRD analysis of synthesized Cu-Ni sample: single-phase approach (a) Rietveld refinemented XRD pattern; (b) and (c) enlarged view of the diffraction peaks around 44° and 51.5° 2θ range without peaks split.

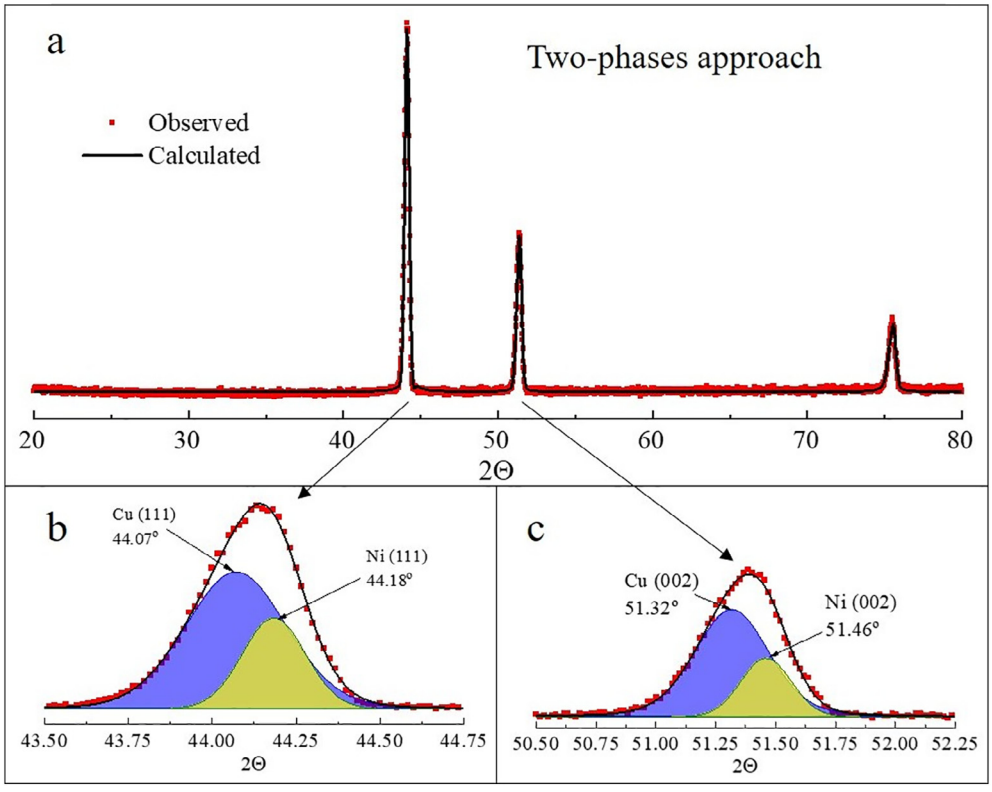

Fig. 6. Results of XRD analysis of the synthesized Cu-Ni sample: two-phases approach. (a) Rietveld refinemented XRD pattern; (b) and (c) enlarged view of the diffraction peaks around 44° and 51.5° 2θ range, showing peaks split.

Table 2
The results of single- and two-phase approaches for Rietveld refinement of phase content, lattice parameters, and particle size of SCS synthesized Cu-Ni powder.

Approach	Composition	Space group	a, Å	Cell volume, Å^3	d, nm	R_p	GoF
Single-phase	$Cu_{0.502}Ni_{0.498}$	Fm-3 m	3.5698	45.49115	30	3.83	1.277
Two-phases	Cu = 52.1%	Fm-3 m	3.5689	45.45719	29	3.85	1.298
	Ni = 47.9%	Fm-3 m	3.5584	45.05730	55		

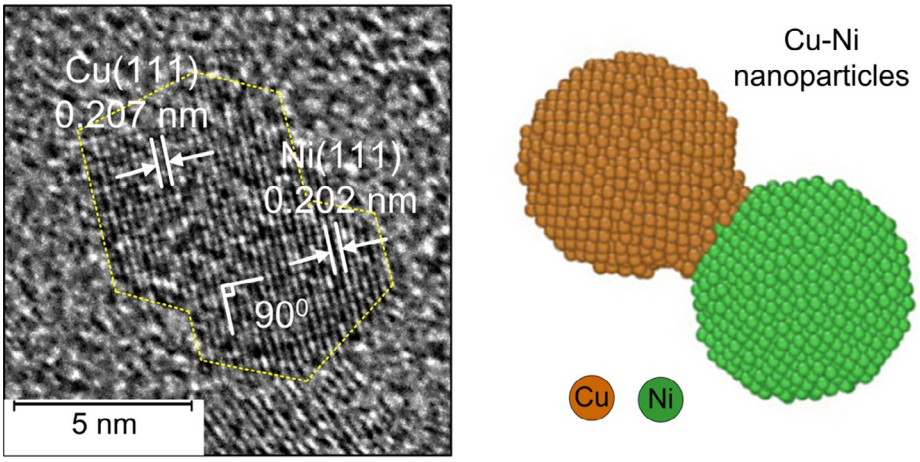

Fig. 7. HR-TEM image of SCS Cu-Ni sample.

Table 3
Temperature dependence of the dihedral angle $< \psi >$ and neck radius $< R >$ of the system Cu-Ni without initial distance (a standard deviation of the dihedral angle σ).

T, K	$< \psi >$, °	σ, °	$< R >$, nm
300	105.02	4.84	0.80
340	116.01	6.24	0.88
380	127.96	6.34	0.96
420	132.29	5.99	1.01
460	136.44	6.99	1.05
500	137.40	4.81	1.40
540	137.51	4.40	1.41

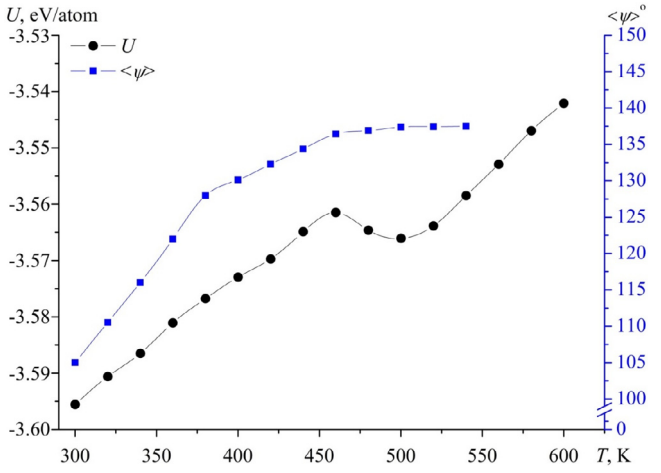

Fig. 8. The temperature dependences of (black curve) the potential part of the internal energy of the system and (blue curve) the dihedral angle of the neck – the Cu-Ni system at an initial distance of 0.0 nm. The black curve bend at 460 K corresponds to the start of the surface relaxation of the nanoparticle.

The fourth stage starts at the temperature of about 356 °C, where the afterburning process continues in a smoldering mode. Thus, the temperature value of 500 °C was chosen for SCS of Cu-Ni NPs to guaranty the finishing of all active combustion processes.

3.2. Characterization of synthesized Cu-Ni NPs

Fig. 4 shows SEM images and results of the EDS element mapping of the SCS obtained powder. From the SEM images, one could see the microstructure of the experimental sample consists of highly porous thin flakes and dendritic agglomerates (Fig. 4a). The image with an enlarged view of the powder (Fig. 4b) shows the agglomerates consist of mush smaller crystals, which could not be clearly distinguished on such level of magnification.

The observed porous structure of agglomerated nanocrystals is typical for materials, obtained by the SCS approach and one of its features. The dendritic structure forms due to the nature of the combustion process, where local gradients of temperature and components' concentration cause local self-propagated combustion waves, while overall the SCS process occurs in a volume explosion mode. At the same time, a large volume of gases evaluates as a result of precursor decomposition, which also influences the microstructure of the powder and, mainly, its high porosity.

The results of the EDS element mapping study (Fig. 4c) show the synthesized material consists of Cu (44.89 wt%), Ni (52.43 wt%), and O (2.68 wt%) atoms distributed homogeneously across the sample. The higher content of nickel atoms could indicate, the grains of the samples have a core–shell type structure with more Ni atoms concentrated closer to their surfaces. At the same time, separate pure Cu and Ni grains were not founded. The presence of oxygen atoms indicates the formation of tine oxide film on the surface of metallic grains, which is common for metal nanopowders.

Figs. 5 and 6, and Table 2 show results of XRD analysis of SCS synthesized nanomaterials, where single-phase and two-phases Rietveld refinement approaches, respectively, were used.

Based on the results of the single-phase XRD pattern analysis (Fig. 5a) it could be seen that the sample is pure bimetallic nanopowder with the stoichiometric composition $Cu_{0.502}Ni_{0.498}$ in cubic (Fm-3 m

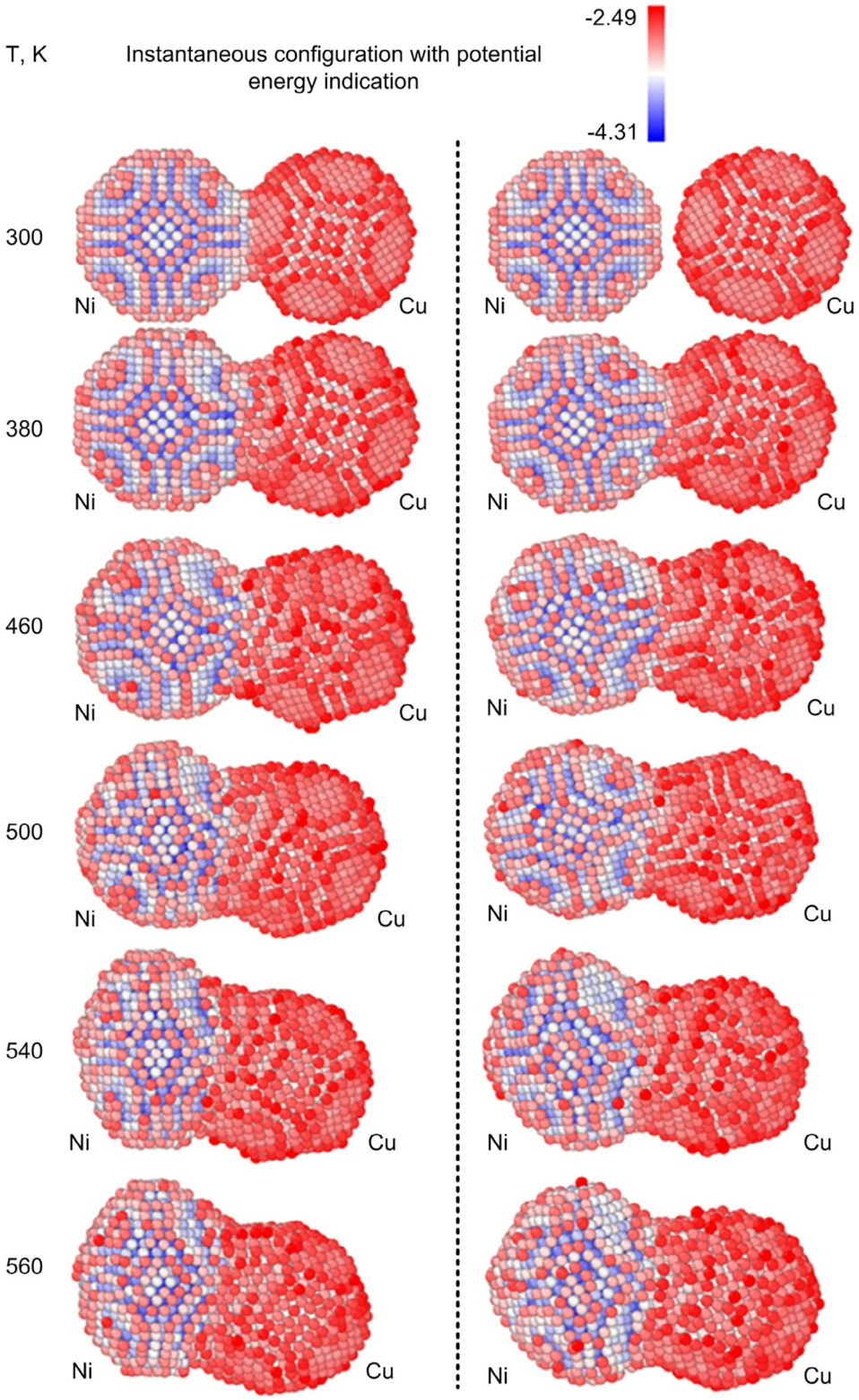

Fig. 9. Instantaneous system configurations with potential energy indication of the Cu-Ni (left is initial distance 0.0 nm, right is an initial distance of 0.2 nm).

space group) crystal phase. The characteristic XRD peaks (1 1 1), (0 0 2), and (0 2 2) were detected at 44.11°, 51.36°, and 75.47°, respectively, which are middle values between cubic Cu and Ni crystal phases. The enlarged view on (1 1 1) and (0 0 2) peaks (Fig. 5b and c) shows the good quality of peaks feating, which confirms by the goodness-of-feat coefficient (GoF) value of 1.277. The calculated crystalline size of the single-phase bimetallic CuNi phase is 30 nm.

Analysis of the results of two-phases Rietveld refinement approach (Fig. 6a) shows the SCS synthesized nanomaterial consists of two mutually distorted separate crystal phases of cubic (Fm-3 m space group) Cu and Ni with characteristic peaks (1 1 1), (0 0 2), and (0 2 2) at 44.07°, 51.32° and 75.41° for Cu phase, and 44.18°, 51.46° and 75.68° for Ni phase, respectively. No other crystalline phases were detected in the diffraction patterns. The peaks of the two phases are significantly

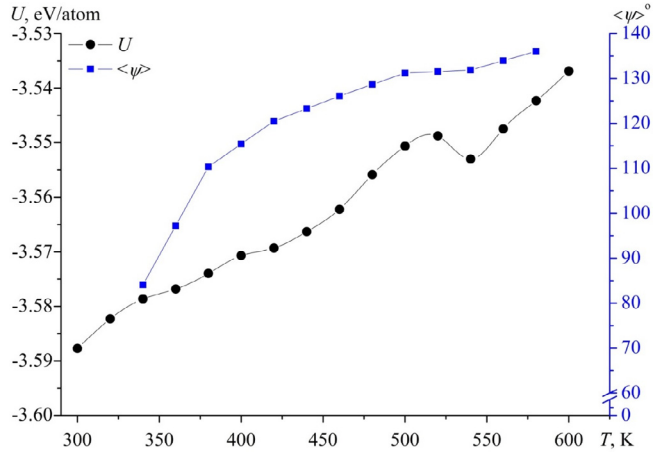

Fig. 10. The temperature dependences of (black curve) the potential part of the specific internal energy of the system and (blue curve) the average dihedral angle of the neck – the Cu-Ni system at an initial distance of 0.2 nm. The black curve bend at 540 K corresponds to the start of the surface relaxation of the nanoparticle.

Table 4
The calculated values of the dihedral angle and radius of the neck of the Cu-Ni system with an initial distance of 0.2 nm at different temperatures.

T, K	$< \psi >$, °	σ, °	$< R >$, nm
300	–	–	–
340	84.09	5.22	0.39
380	110.35	6.85	0.66
420	120.52	8.43	0.79
460	126.09	8.55	0.87
500	131.22	7.21	0.93
540	131.89	7.64	1.31

shifted from parameters of Cu and Ni synthesized by the same SCS method before [39,40]. The calculated crystalline sizes of Cu and Ni phases are 29 nm and 55 nm, respectively. The enlarged view on (1 1 1) and (0 0 2) peaks (Fig. 6b and c) shows the good quality of peaks feat, with the GoF coefficient of 1.298, which is almost the same as for single-phase refinemented XRD pattern.

Based on the comparison of the refinement results for both approaches we can conclude, that the only XRD pattern analysis could not indicate the preferable form of the crystallization of synthesized Cu-Ni nanomaterial due to close crystalline parameters of the single- and two-phase forms. Such close calculated parameters along with almost the same GoF values may indicate, that the NPs are in the intermediate state between two- and single-phase form.

The results of a more detailed study of the SCS Cu-Ni sample are presented in Fig. 7. In the HR-TEM image (Fig. 7a) the small double-crystal grain of around 5 nm width for each crystal is seen. The calculated d-spacing values of 0.207 nm and 0.202 nm show the grain consists of one Cu (upper) and one Ni (bottom) crystal, which corresponds to the two-phases model (Fig. 7b).

According to the binary phase diagram, Cu and Ni form a continuous range of solid solutions. However, from the presented experimental data, one can conclude that the synthesized nanopowders are bimetallic particles with cointegrated individual crystal structures of nickel and copper. We suppose, such a structure could originate in the process of crystallization of individual Cu and Ni grains with subsequent interaction at high temperatures during SCS. Because of kinetic limitations, the particles' interaction time is not enough for the finished formation of solid solution bimetallic nanoparticle at the existent synthesis temperature. In its' turn, the metal phase separation could occur at the drying stage, due to different stability of Cu and Ni ions in the G-containing solution. The results of the modeling of bimetallic nanoparticle formation in case of interaction of two separate nanoparticles are presented below.

3.3. Simulation results

Table 3 shows the parameters of the forming neck in the nanoalloy Cu-Ni and Fig. 8 shows the temperature dependences of the potential part of the internal energy of the system simultaneously with the temperature dependences of the dihedral angle. The temperature range for the simulation is 300–600 K. The value of the dihedral angle ψ and a standard deviation of the dihedral angle σ were determined by the method described in [46] and the average value $< \psi >$ in all directions of the neck is presented in the Fig. 9.

It can be noted that the curve of the potential part of the internal energy up to 460 K corresponds to the growth of the neck and the surface relaxation refers to a change in the position of surface atoms. However, the diffusion processes in the neck at that temperature range do not result in significant mixing of the sorts of atoms. Furthermore, following temperature increase leads to some decrease of the potential part of the internal energy, which means the energy state of the system, including neck, becomes unfavorable, and the growth of the dihedral angle temporarily stops. A small temperature increase of only about 10–15 K leads to continuing of dihedral angle growth, and the system passes through a stable state corresponding to 500 K. The further dihedral angle growth and the increase in the potential part of the internal energy are associated with intensive diffusion processes, significant particles shape change, and, finally, the formation of cointegrated Co-Ni single particle. Fig. 9 shows the energetic evolution of the system with the different initial distance between Cu and Ni nanoparticles in general and, specifically, the transformation of the neck in the transition zone. The comparison indicates that in the case of initial contact, the deformation of the boundary of integrated Cu-Ni nanoparticle is more pronounced. This leads to a slightly different energy spectrum of both internal atoms and shell atoms.

Fig. 10 and Table 4 show the results of the simulation for the initial configuration case with the distance between the Cu-Ni nanoparticles of 0.2 nm. A distinctive feature of this case, in comparison with the case with the distance between nanoparticles of 0.0 nm, is «delayed» by the 60–80 K coalescence process. The delay appears due to the need for the particles to move closer to begin the process of forming a stable neck.

However, the temperature curves of the potential part of the internal energy of this system and the dihedral angle of the neck also indicate the existence of energetically stable stages of neck formation and the possibility of further evolution of the system. The presence of a distance between nanoparticles at the initial time moment affects the energy distribution of atoms and the fraction of crystalline structures. Besides, in this case, a more regular symmetric shape is formed at the corresponding final simulation temperature.

From Figs. 8 and 10, one can conclude that the final stage of neck formation for the initial configuration with a gap between the Cu and Ni nanoparticles also «delayed» with the value 30–40 K.

Visualized simulations results, presented in Fig. 9 and Fig. 11, shows an evolution in the energy spectrum and coordination number of the forming neck. In the case of the initial configuration with a gap between nanoparticles, more atoms with lower specific energy are involved in the neck formation process. Also, more atoms correspond to the average value of coordination numbers, formed in the vicinity of the particle contact. In both cases, a buffer zone of atoms with a lower coordination number arises in the neck region. This region expands to the side where nickel atoms were concentrated in the initial stage, at the final stages of coalescence.

The cross-sections of the corresponding systems at different temperatures were calculated for a more detailed study of the local structures, formed in the neck regions and Cu-Ni nanoparticle (Fig. 12). It could be seen, at the initial stage the bcc phase forms with an interlayer

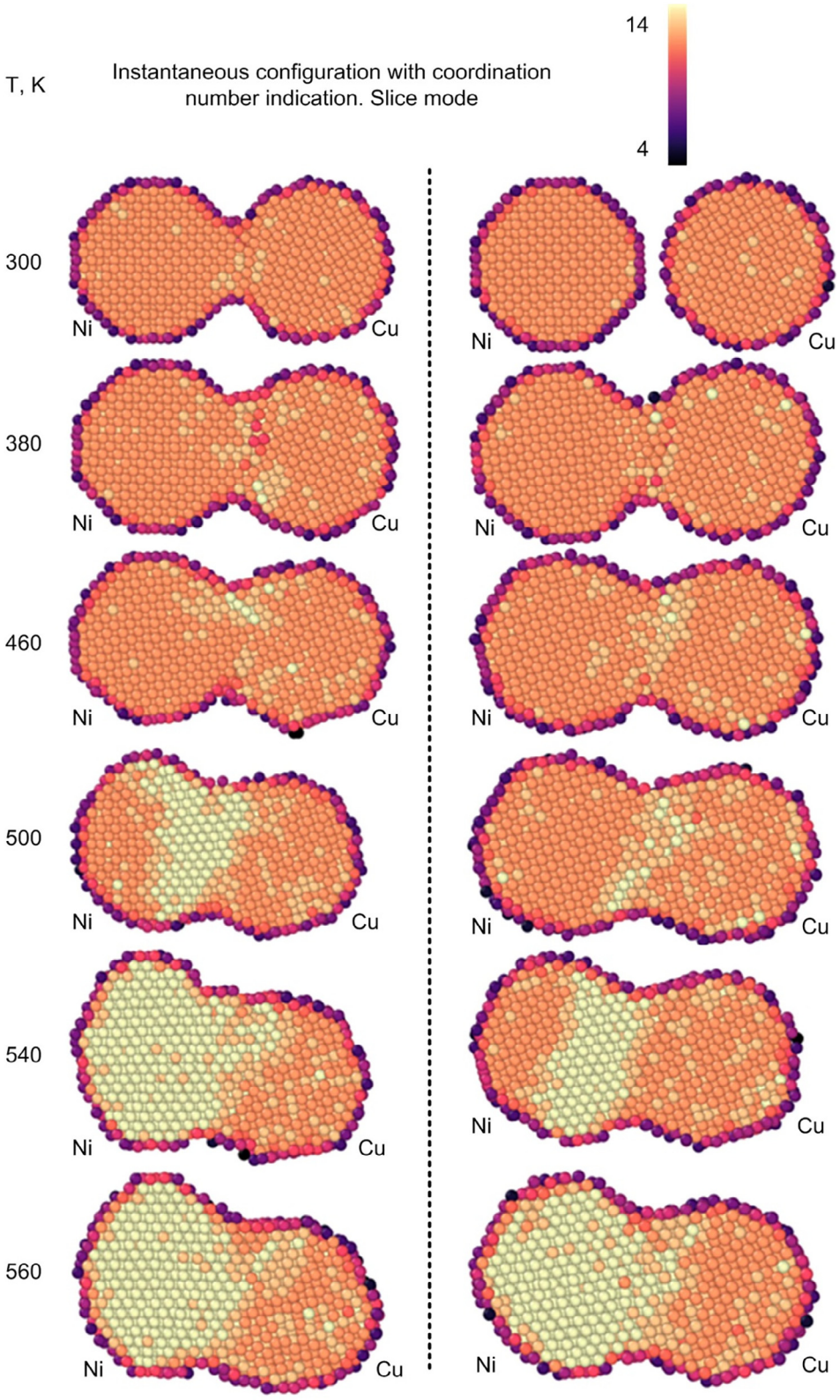

Fig. 11. Instantaneous system configurations with coordination number indication of the Cu-Ni (left is initial distance 0.0 nm, right is the initial distance of 0.2 nm).

of the hcp phase. Then the bcc phase spreads to all Ni atoms and part of the internal Cu atoms. At the same time, the cross-sections of the corresponding systems are quite similar at 540 K. Thus, we can conclude that the distance between Cu-Ni nanoparticles effects insignificantly on the final configurations. However, it can influence the initial and intermediate stages of the neck formation process. It is noteworthy that the formation of zonal/band structures was detected both in-silico [50] and in experimental studies [51]. Moreover, these zonal/band structures can arise not only in the region of the neck formation but also in regions mainly containing a certain sort of initial metal atoms.

The simulation data confirm the possible absence of the significant mixing in the system at T below 500 K in case of the formation of

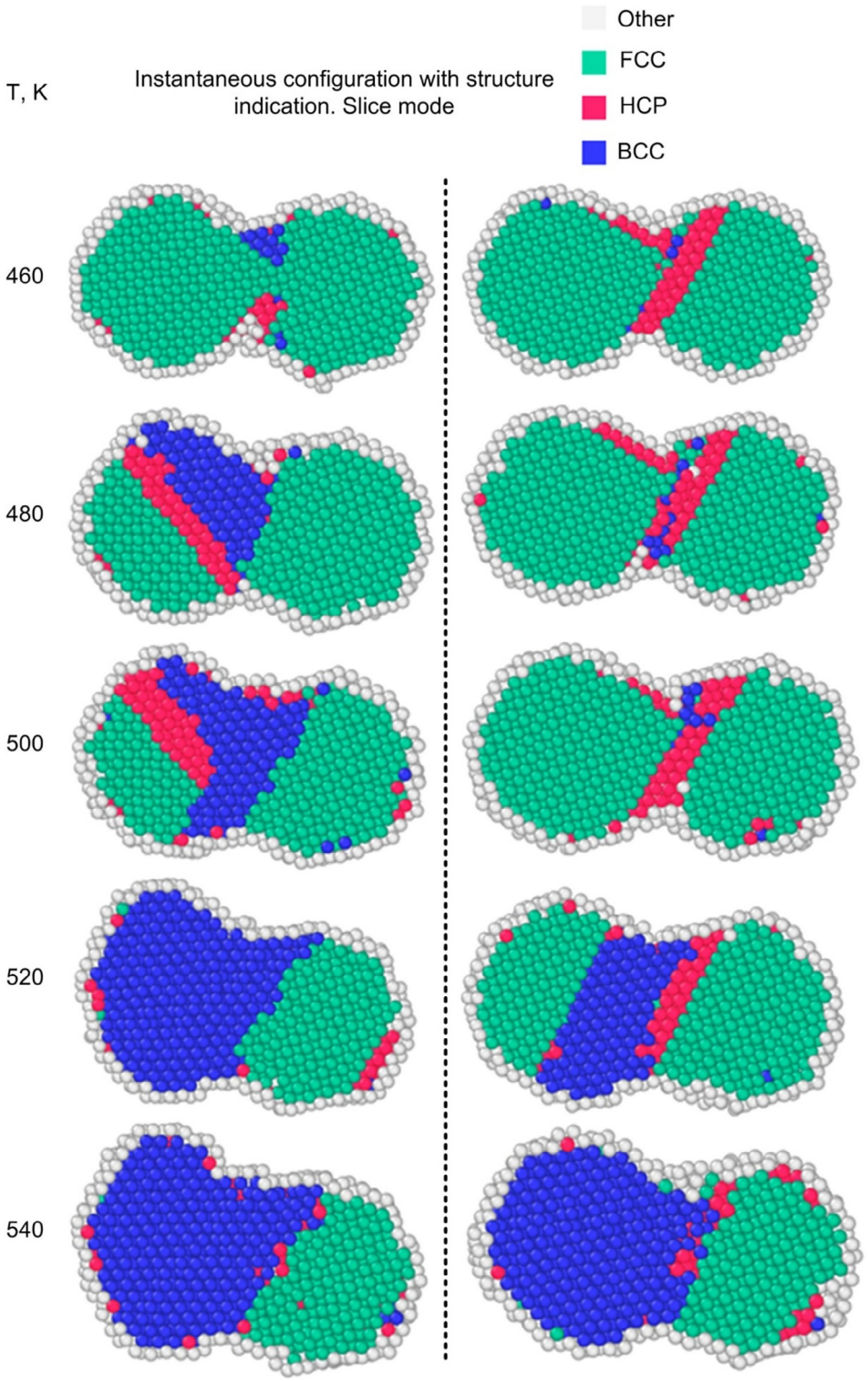

Fig. 12. Instantaneous configuration with structure indication of the Cu-Ni (left is initial distance 0.0 nm, right is an initial distance of 0.2 nm).

bimetallic nanoparticle starting from the two separate nanoparticles of Cu and Ni.

Comparison of the data obtained during computer simulation and the results of studying of SCS nanoparticles (Fig. 7) shows the Cu and Ni particles were formed independently during combustion, and then, start to cointegrate, which indicates by the relatively regular shape of Cu-Ni nanoparticle.

However, the existence of both mechanisms in such a complex system as an SCS reaction is possible. Also, we can conclude, the possibility of predicting the resulting structures forming during the synthesis to estimate the energy of the grain boundary and the dihedral angle. Besides, it can be useful for predicting the energy spectrum of particles as well as possible stable structural compositions inside bimetallic Cu-Ni nanoparticles. The approach could be used for developing compositions and effective methods for the synthesis of polymetallic nanomaterials for catalysts, sensors, and other applications.

4. Conclusions

The bimetallic nanoparticles were successfully synthesized by a modified SCS approach and characterized by various methods. The study showed the synthesized particles are fine interconnected Cu-Ni metallic crystallites. The Monte-Carlo simulations of particles' formation process showed the possibility of the different initial configuration of the neck and the particle's mutual arrangement, leading to various possible final energy allowable configurations with a variety of crystalline phases. It was found, that increasing temperature after neck formation could lead to segregation phenomena in nanoparticles, the intensity of which will depend on the difference in the surface energy of Cu and Ni crystallites. The founded possibility for the formation of bimetallic nanoparticles from different mutual initial configurations demonstrates the possibility of creating both spatially symmetric and asymmetric structures. The described approach and results of the study could be used for developing compositions and effective methods for the synthesis of polymetallic nanomaterials for catalysts, sensors, and other applications.

CRediT authorship contribution statement

Nickolay Sdobnyakov: Conceptualization, Methodology, Data curation. **Alexander Khort:** Conceptualization, Validation, Formal analysis, Investigation, Data curation, Writing - review & editing, Visualization. **Vladimir Myasnichenko:** Software, Formal analysis. **Kirill Podbolotov:** Investigation, Data curation. **Elena Romanovskaia:** Data curation. **Andrey Kolosov:** Visualization, Investigation. **Denis Sokolov:** Software, Validation. **Valentin Romanovski:** Conceptualization, Validation, Formal analysis, Investigation, Data curation, Writing - review & editing, Visualization.

Declaration of Competing Interest

The authors declare that they have no known competing financial interests or personal relationships that could have appeared to influence the work reported in this paper.

Acknowledgments

This work was supported by the Ministry of Science and Higher Education of the Russian Federation in the framework of Increase Competitiveness Program of NUST «MISiS» (№ K2-2019-007), implemented by a governmental decree dated 16th of March 2013, N 211; and in the framework of the State Program in the Field of the Research Activity (project number 0817-2020-0007). The reported study was funded by RFBR, projects number 20-37-70007, and 18-03-00132. This work also was supported by the Swedish Foundation for Strategic Environmental Research through the MISTRA Environmental Nanosafety program.

References

[1] P. Srinoi, Y.T. Chen, V. Vittur, M.D. Marquez, T.R. Lee, Bimetallic nanoparticles: enhanced magnetic and optical properties for emerging biological applications, Appl. Sci. 8 (7) (2018) 1106, https://doi.org/10.3390/app8071106.
[2] J. Rick, M.C. Tsai, B.J. Hwang, Biosensors incorporating bimetallic nanoparticles, Nanomaterials 6 (1) (2016) 5, https://doi.org/10.3390/nano6010005.
[3] M. Khatami, H.Q. Alijani, I. Sharifi, Biosynthesis of bimetallic and core–shell nanoparticles: their biomedical applications–a review, IET Nanobiotechnol. 12 (7) (2018) 879–887, https://doi.org/10.1049/iet-nbt.2017.0308.
[4] K. Loza, M. Heggen, M. Epple, Synthesis, structure, properties, and applications of bimetallic nanoparticles of noble metals, Adv. Funct. Mater. 1909260 (2020), https://doi.org/10.1002/adfm.201909260.
[5] X. Liu, D. Wang, Y. Li, Synthesis and catalytic properties of bimetallic nanomaterials with various architectures, Nano Today 7 (5) (2012) 448–466.
[6] N. Toshima, T. Yonezawa, Bimetallic nanoparticles – novel materials for chemical and physical applications, New J. Chem. 22 (11) (1998) 1179–1201.
[7] V.M. Samsonov, I.V. Talyzin, A.Y. Kartoshkin, S.A. Vasilyev, Surface segregation in binary Cu-Ni and Au-Co nanoalloys and the core–shell structure stability/instability: thermodynamic and atomistic simulations, Appl. Nanosci. 9 (1) (2019) 119–133, https://doi.org/10.1007/s13204-018-0895-5.
[8] Kolosov A.Yu., Sokolov D.N., Sdobnyakov N.Yu., Komarov P.V., Bogdanov S.S., Bogatov A.A., Myasnichenko V.S. (2017). Estimation of the dihedral angle between metal nanoparticles during their coalescence. Journal of Nano- and Electronic Physics, 9(5), 05042-1 - 05042-4. doi.org/10.21272/jnep.9(5).05042.
[9] A.Y. Kolosov, N.Y. Sdobnyakov, V.S. Myasnichenko, D.N. Sokolov, Investigation into the structure and features of the coalescence of differently shaped metal nanoclusters, J. Surf. Invest. 10 (6) (2016) 1292–1299, https://doi.org/10.1134/S102745101605075X.
[10] S. Haeri, L. Benedetti, O. Ghita, Effects of particle elongation on the binary coalescence dynamics of powder grains for Laser Sintering applications, Powder Technol. 363 (2020) 245–255, https://doi.org/10.1016/j.powtec.2019.12.025.
[11] F. Qiu, T.A. Egerton, I.L. Cooper, Monte Carlo simulation of nano-particle sintering, Powder Technol. 182 (115) (2008) 42–50, https://doi.org/10.1016/j.powtec.2007.05.007.
[12] L. Benedetti, B. Brulé, N. Decraemer, K.E. Evans, O. Ghita, Methods for evaluating particle coalescence and their implications in laser sintering, Powder Technol. 342 (2019) 917–928, https://doi.org/10.1016/j.powtec.2018.10.053.
[13] M.H. Aghaali, S. Firoozi, Synthesis of nanostructured fcc/hcp hollow Ni particles by ultrasonic spray pyrolysis and its dry reforming catalytic properties //, Powder Technol. 356 (2019) 119–128, https://doi.org/10.1016/j.powtec.2019.08.023.
[14] L. Argueta-Figueroa, R.A. Morales-Luckie, R.J. Scougall-Vilchis, O.F. Olea-Mejía, Synthesis, characterization and antibacterial activity of copper, nickel and bimetallic Cu–Ni nanoparticles for potential use in dental materials, Progr. Natural Sci.: Mater. Int. 24 (4) (2014) 321–328, https://doi.org/10.1016/j.pnsc.2014.07.002.
[15] J. Chaudhary, G. Tailor, B.L. Yadav, O. Michael, Synthesis and biological function of Nickel and Copper nanoparticles, Heliyon 5 (6) (2019) e01878, , https://doi.org/10.1016/j.heliyon.2019.e01878.
[16] S.M. Pudi, P. Biswas, S. Kumar, B. Sarkar, Selective hydrogenolysis of glycerol to 1, 2-propanediol over bimetallic Cu-Ni Catalysts supported on γ-Al2O3, J. Braz. Chem. Soc. 26 (8) (2015) 1551–1564.
[17] B. Seemala, C.M. Cai, R. Kumar, C.E. Wyman, P. Christopher, Effects of Cu–Ni bimetallic catalyst composition and support on activity, selectivity, and stability for furfural conversion to 2-methyfuran, ACS Sustainable Chem. Eng. 6 (2) (2018) 2152–2161, https://doi.org/10.1021/acssuschemeng.7b03572.
[18] S.A. Hashemizadeh, M. Biglari, Cu: Ni bimetallic nanoparticles: facile synthesis, characterization and its application in photodegradation of organic dyes, J. Mater. Sci.: Mater. Electron. 29 (15) (2018) 13025–13031, https://doi.org/10.1007/s10854-018-9424-2.
[19] S. Rana, S.B. Jonnalagadda, A facile synthesis of Cu–Ni bimetallic nanoparticle supported organo functionalized graphene oxide as a catalyst for selective hydrogenation of p-nitrophenol and cinnamaldehyde, RSC Adv. 7 (5) (2017) 2869–2879, https://doi.org/10.1039/C6RA26443C.
[20] D. Mukherjee, R. Singuru, P. Venkataswamy, D. Damma, B.M. Reddy, Ceria promoted Cu-Ni/SiO2 catalyst for selective hydrodeoxygenation of vanillin, ACS Omega 4 (3) (2019) 4770–4778, https://doi.org/10.1021/acsomega.9b00039.
[21] G. Mayakrishnan, V. Elayappan, I.S. Kim, I.M. Chung, Sea-island-like morphology of CuNi bimetallic nanoparticles uniformly anchored on single layer graphene oxide as a highly efficient and noble-metal-free catalyst for cyanation of aryl halides, Sci. Rep. 10 (1) (2020) 1–15, https://doi.org/10.1038/s41598-020-57483-z.
[22] Z. Bian, S. Das, M.H. Wai, P. Hongmanorom, S. Kawi, A review on bimetallic nickel-based catalysts for CO2 reforming of methane, ChemPhysChem 18 (22) (2017) 3117–3134, https://doi.org/10.1002/cphc.201700529.
[23] G.H. Mohamed Saeed, S. Radiman, S.S. Gasaymeh, H.N. Lim, N.M. Huang, Mild hydrothermal synthesis of Ni–Cu nanoparticles, J. Nanomater. 2010 (2010), https://doi.org/10.1155/2010/184137.
[24] J. Ahmed, K.V. Ramanujachary, S.E. Lofland, A. Furiato, G. Gupta, S.M. Shivaprasad, A.K. Ganguli, Bimetallic Cu–Ni nanoparticles of varying composition (CuNi3, CuNi, Cu3Ni), Colloids Surf., A 331 (3) (2008) 206–212, https://doi.org/10.1016/j.colsurfa.2008.08.007.
[25] I. Ban, J. Stergar, M. Drofenik, G. Ferk, D. Makovec, Synthesis of copper–nickel nanoparticles prepared by mechanical milling for use in magnetic hyperthermia, J. Magn. Magn. Mater. 323 (17) (2011) 2254–2258, https://doi.org/10.1016/j.jmmm.2011.04.004.
[26] G.R. Rao, S.K. Meher, B.G. Mishra, P.H.K. Charan, Nature and catalytic activity of bimetallic CuNi particles on CeO2 support, Catal. Today 198 (2012) 140–147, https://doi.org/10.1016/j.cattod.2012.06.027.
[27] N. Riaz, F.K. Chong, B.K. Dutta, Z.B. Man, M.S. Khan, E. Nurlaela, Photodegradation of Orange II under visible light using Cu–Ni/TiO2: effect of calcination temperature, Chem. Eng. J. 185–186 (2012) 108–119, https://doi.org/10.1016/j.cej.2012.01.052.
[28] D. Wu, Q. Tan, L. Hu, Shape-controlled synthesis of Cu-Ni nanocrystals, Mater. Chem. Phys. 206 (2018) 150–157, https://doi.org/10.1016/j.matchemphys.2017.12.013.
[29] C. Tojo, D. Buceta, M.A. López-Quintela, On metal segregation of bimetallic nanocatalysts prepared by a one-pot method in microemulsions, Catalysts 7 (2) (2017) 68, https://doi.org/10.3390/catal7020068.
[30] H.H. Brongersma, M.J. Sparnaay, T.M. Buck, Surface segregation in Cu-Ni and Cu-Pt alloys; a comparison of low-energy ion-scattering results with theory, Surf. Sci. 71 (3) (1978) 657–678, https://doi.org/10.1016/0039-6028(78)90453-3.
[31] M. Hennes, J. Buchwald, U. Ross, A. Lotnyk, S.G. Mayr, Equilibrium segregation patterns and alloying in Cu/Ni nanoparticles: experiments versus modeling, Phys. Rev. 91 (2015) 245401-1–245401-11, https://doi.org/10.1103/PhysRevB.91.245401.

[32] F. Cleri, V. Rosato, Tight-binding potentials for transition metals and alloys, Phys. Rev. B 48 (1) (1993) 22–33, https://doi.org/10.1103/PhysRevB.48.22.
[33] E. Panizon, J. Olmos-Asar, M. Peressi, R. Ferrando, The study of the structure and thermodynamics of CuNi nanoalloys using a new DFT-fitted atomistic potential, PCCP 17 (42) (2015) 28068–28075, https://doi.org/10.1039/C5CP00215J.
[34] G. Xanthopoulou, G. Vekinis, An overview of some environmental applications of self-propagating high-temperature synthesis, Adv. Environ. Res. 5 (2) (2001) 117–128, https://doi.org/10.1016/S1093-0191(00)00048-4.
[35] A. Varma, A.S. Mukasyan, A.S. Rogachev, K.V. Manukyan, Solution combustion synthesis of nanoscale materials, Chem. Rev. 116 (23) (2016) 14493–14586, https://doi.org/10.1021/acs.chemrev.6b00279.
[36] V.V. Romanovskii, A.A. Khort, K.B. Podbolotov, N.Y. Sdobnyakov, V.S. Myasnichenko, D.N. Sokolov, One-step synthesis of polymetallic nanoparticles in air invironment, Izv. Vyssh. Uchebn. Zaved., Khim. Khim. Tekhnol. 61 (9–10) (2018) 42–47, https://doi.org/10.6060/ivkkt.20186109-10.5867a.
[37] V.I. Romanovskii, A.A. Khort, Modified anthracites for deironing of underground water, J. Water Chem. Technol. 39 (5) (2017) 299–304, https://doi.org/10.3103/S1063455X17050083.
[38] D. Propolsky, E. Romanovskaia, W. Kwapinski, V. Romanovski, Modified activated carbon for deironing of underground water, Environ. Res. 182 (2020) 108996, , https://doi.org/10.1016/j.envres.2019.108996.
[39] A.A. Khort, K.B. Podbolotov, R. Serrano-García, Y.K. Gun'ko, One-step solution combustion synthesis of pure Ni nanopowders with enhanced coercivity: the fuel effect, J. Solid State Chem. 253 (2017) 270–276, https://doi.org/10.1016/j.jssc.2017.05.043.
[40] K.B. Podbolotov, A.A. Khort, A.B. Tarasov, G.V. Trusov, S.I. Roslyakov, A.S. Mukasyan, Solution combustion synthesis of copper nanopowders: the fuel effect, Combust. Sci. Technol. 189 (11) (2017) 1878–1890, https://doi.org/10.1080/00102202.2017.1334646.
[41] N. Metropolis, S. Ulam, The Monte Carlo method, J. Am. Stat. Assoc. 44 (247) (1949) 335–341.
[42] R.P. Gupta, Lattice relaxation at a metal surface, Phys. Rev. B. 23 (12) (1981) 6265–6270, https://doi.org/10.1103/PhysRevB.23.6265.
[43] H. Chamati, N.I. Papanicoluou, Second-moment interatomic potential for gold and its application to molecular-dynamics simulations, J. Phys.: Condens. Matter 16 (46) (2004) 8399–8407, https://doi.org/10.1088/0953-8984/16/46/025.
[44] N.T. Wilson, R.L. Johnson, A theoretical study of atom ordering in copper-gold nanoalloy clusters, J. Mater. Chem. 12 (10) (2002) 2913–2922, https://doi.org/10.1039/B204069G.
[45] L.O.P. Borbon, Computational Studies of Transition Metal Nanoalloys, Berlin Heidelberg Springer-Verlag, XVI, 2011, p. 156.
[46] Kolosov A.Yu., Sokolov D.N., Sdobnyakov N.Yu., Komarov P.V., Bogdanov S.S., Bogatov A.A., Myasnichenko V.S. (2017). Estimation of the dihedral angle between metal nanoparticles during their coalescence. Journal of Nano- and Electronic Physics, 9 (5), 05042-1 - 05042-4.
[47] P. Grammatikopoulos, E. Toulkeridou, K. Nordlund, M. Sowwan, Simple analytical model of nanocluster coalescence for porous thin film design, Modell. Simul. Mater. Sci. Eng. 23 (1) (2015) 015008, , https://doi.org/10.1088/0965-0393/23/1/015008.
[48] A. Khort, K. Podbolotov, R. Serrano-García, Y. Gun'ko, One-step solution combustion synthesis of cobalt nanopowder in air atmosphere: the fuel effect, Inorg. Chem. 57 (3) (2018) 1464–1473, https://doi.org/10.1021/acs.inorgchem.7b02848.
[49] A. Khort, V. Romanovski, V. Lapitskaya, T. Kuznetsova, Kh. Yusupov, D. Moskovskikh, Yu. Haiduk, K. Podbolotov, Graphene@metal nanocomposites by solution combustion synthesis, Inorg. Chem. 59 (9) (2020) 6550–6565, https://doi.org/10.1021/acs.inorgchem.0c00673.
[50] D.N. Sokolov, A.P. Andriychuk, M.P. Kharitonova, I.V. Kartashov, P.V. Komarov, N.Yu. Sdobnyakov, The investigation of the structural characteristics of the metal nanoclusters in melting/crystallization process using many-body Gupta potential, Physical and chemical aspects of the study of clusters, nanostructures and nanomaterials 5 (2013) 301–316.
[51] Perevezentsev V.N. (1995) The theory of evolution of the microstructure of superplastic alloys and ceramics; N. Ridley (ed.), in Superplasticity. 60 years after Pearson. London: Bourne Press, 51-59.